that the radiation of the Whiterock trilobite fauna was initiated in more offshore settings than that of the Paleozoic Fauna.

In assessing the reasons for the differing responses of trilobite groups during the Ordovician radiation, it will ultimately be necessary to understand their early phylogenetic history. Many problems remain in resolving trilobite relationships across the Cambro-Ordovician boundary (*34*). However, it is principally Ibex Fauna families that have known or suspected Cambrian distributions. Whiterock Fauna families, and in particular Silurian Fauna groups, can generally be traced only to the Early Ordovician, and in many cases they are entirely "cryptogenetic." These clades certainly had Cambrian forebears, but the fact that they have avoided detection is a strong indication that novel morphologies were being developed very rapidly. This implied difference in rates of evolution is testable through analysis of species turnover, and is perhaps the most compelling clue to the strikingly disjunct fates of post-Cambrian trilobites.

REFERENCES AND NOTES

1. A. T. Thomas and R. A. Fortey, in *Atlas of Invertebrate Macrofossils,* J. W. Murray, Ed. (Longman, London, 1985), pp. 199–229; R. A. Robison, in *Fossil Invertebrates*, R. S. Boardman, A. H. Cheetham, A. J. Rowell, Eds. (Blackwell, Palo Alto, CA, 1987), pp. 221–241.
2. J. J. Sepkoski Jr., *Milwaukee Public Mus. Contrib. Biol. Geol.* **83**, 1 (1992).
3. The full data set has not yet been published, but preliminary plots are given by J. J. Sepkoski Jr., in (*22*), pp. 393–396.
4. ——, *Paleobiology* **7**, 36 (1981).
5. R. A. Fortey, D. E. G. Briggs, M. A. Wills, *Bioessays* **19**, 429 (1997).
6. M. L. Droser, R. A. Fortey, X. Li, *Am. Sci.* **84**, 122 (1996).
7. P. J. Brenchley, in *Mass Extinctions: Processes and Evidence*, S. K. Donovan, Ed. (Belhaven, London, 1990), pp. 104–132.
8. R. A. Fortey and R. M. Owens, in *Major Evolutionary Radiations*, P. D. Taylor and G. P. Larwood, Eds. (Systematics Association Special Volume 42, Clarendon, Oxford, 1990), pp. 139–164.
9. M. Foote, *Paleobiology* **14**, 258 (1988).
10. S. J. Culver, M. A. Buzas, L. S. Collins, *ibid.* **13**, 169 (1987).
11. The full database will be published elsewhere; a current version is available from the senior author on request.
12. We used North American Ordovician series, but the globally correlative *Nemograptus gracilis* Zone is included in the Mohawk, instead of its traditional assignment to the upper Whiterock. This revision is based on the recent recommendations of the Subcommission on Ordovician Stratigraphy and results in more satisfactory sampling intervals. At the series level of resolution, there are few examples of Lazarus taxa (taxa occurring earlier and later than, but not within, a given sampling interval); where such sampling gaps occurred, genera were scored as present.
13. Principal components analysis of the data set confirmed the division into two major faunas. The groupings are so robust that the use of alternative similarity indices will not significantly alter the result.
14. A single family, Harpetidae, falls outside the two major clusters. The generic taxonomy of this group is in need of revision.
15. We define the Silurian Fauna as Whiterock Fauna families in which at least one lineage survived the end-Ordovician extinction and subsequently diversified, thus excluding two minor relict distributions, Pterygometopidae and Raphiophoridae, in each of which a single low-diversity lineage extended into the Silurian but became extinct during the period.
16. Upper Arenig in British terminology.
17. M. E. Patzkowsky, in (*22*), pp. 413–414.
18. R. L. Anstey and J. F. Pachut, in *New Approaches to Speciation in the Fossil Record*, D. H. Erwin and R. L. Anstey, Eds. (Columbia Univ. Press, New York, 1995), pp. 239–284.
19. J. C. W. Cope, *Palaeontology* **39**, 979 (1996); *ibid.* **40**, 713 (1997); J. Pojeta and J. Gilbert-Tomlinson, *Bull. Bur. Miner. Res. Geol. Geophys.* **174**, 1 (1977).
20. J. Sprinkle, in *Origins and Early Evolution of the Metazoa*, J. H. Lipps and P. W. Signor, Eds. (Plenum, New York, 1992), pp. 375–398.
21. R. A. Fortey and R. A. Cooper, *Palaeontology* **29**, 631 (1986).
22. M. L. Droser, P. M. Sheehan, R. A. Fortey, X. Li, in *Ordovician Odyssey: Short Papers for the Seventh International Symposium on the Ordovician System*, J. D. Cooper, M. L. Droser, S. C. Finney, Eds. (Pacific Section Society for Sedimentary Geology, Fullerton, CA, 1995), pp. 405–408.
23. J. J. Sepkoski Jr., in *Short Papers for the Second International Symposium on the Cambrian System*, M. E. Taylor, Ed. (USGS Open-File Rep. 81-743, 1981), pp. 203–207.
24. D. Jablonski, *Science* **231**, 129 (1986).
25. D. H. Erwin, *Paleobiology* **16**, 187 (1990).
26. S. R. Westrop, *ibid.* **15**, 46 (1989).
27. Physical causes of end-Ordovician trilobite extinction were proposed by R. A. Fortey, *Philos. Trans. R. Soc. London Ser. B* **325**, 327 (1989); B. D. E. Chatterton and S. E. Speyer, *Paleobiology* **15**, 118 (1989).
28. J. J. Sepkoski Jr. and A. I. Miller, in *Phanerozoic Diversity Patterns: Profiles in Macroevolution*, J. W. Valentine, Ed. (Princeton Univ. Press, Princeton, 1985), pp. 153–190; J. J. Sepkoski Jr. and P. M. Sheehan, in *Biotic Interactions in Recent and Fossil Benthic Communities*, M. J. S. Tevesz and P. M. McCall, Eds. (Plenum, New York, 1983), pp. 673–717.
29. S. R. Westrop, J. V. Tremblay, E. Landing, *Palaios* **10**, 75 (1995); S. R. Westrop and J. M. Adrain, *Paleobiology* **24**, 1 (1998).
30. Work in progress suggests that this disassociation of clade and alpha diversity continued well into the Silurian [J. M. Adrain, *Geol. Soc. Am. Abstr. Programs* **28**, A291 (1996)].
31. For paleogeographic reconstructions, see W. S. McKerrow and C. R. Scotese, Eds., *Palaeozoic Palaeogeography and Biogeography*, *Geol. Soc. London Mem. 12* (1990).
32. H. B. Whittington, *Bull. Mus. Comp. Zool. Harv. Univ.* **129**, 1 (1963); J. M. Adrain and R. A. Fortey, *Bull. Nat. Hist. Mus. London Geol. Ser.* **53**, 79 (1997).
33. R. A. Fortey and M. L. Droser, *J. Paleontol.* **70**, 73 (1996).
34. H. B. Whittington, *Geol. Mag.* **118**, 591 (1981); R. A. Fortey, *Spec. Pap. Palaeontol.* **30**, 179 (1983); G. D. Edgecombe, in *Extinction and Phylogeny*, M. J. Novacek and Q. D. Wheeler, Eds. (Columbia Univ. Press, New York, 1992), pp. 144–177.

35. We thank G. D. Edgecombe, J. J. Sepkoski Jr., and A. B. Smith for comments on the manuscript. Preparation of this study was funded by Natural Environment Research Council (UK) grant GR3/09654 and by Natural Sciences and Engineering Research Council (Canada) grant 41197.

19 February 1998; accepted 21 April 1998

Visualization of the Local Insulator-Metal Transition in $Pr_{0.7}Ca_{0.3}MnO_3$

Manfred Fiebig,* Kenjiro Miyano, Yoshinori Tomioka, Yasuhide Tokura

The light-induced insulator-metal transition in the "colossal magnetoresistance" compound $Pr_{0.7}Ca_{0.3}MnO_3$ is shown to generate a well-localized conducting path while the bulk of the sample remains insulating. The path can be visualized through a change of reflectivity that accompanies the phase transition. Its visibility provides a tool for gaining insight into electronic transport in materials with strong magnetic correlations. For example, a conducting path can be generated or removed at an arbitrary position just because of the presence of another path. Such manipulation may be useful in the construction of optical switches.

Manganese oxides of the general formula $R_{1-x}A_xMnO_3$ (where R and A are rare- and alkaline-earth ions, respectively) have recently attracted considerable attention because of their unusual magnetic and electronic properties (*1*). In some of these materials, insulator-metal (I-M) transitions can be observed where both conductivity and magnetization change markedly. The $x = 0$ and $x = 1$ end members of the $R_{1-x}A_xMnO_3$ family are insulating and antiferromagnetic (AF) with the Mn ion in the Mn^{3+} and Mn^{4+} state, respectively. For intermediate x, the average Mn valence is non-integer and the material is generally semiconducting or metallic at high temperatures. Most of the perovskite manganites show a ferromagnetic (FM) ground state when the holes are optimally doped (usually $0.2 \leq x \leq 0.5$) by chemical substitution of the perovskite A-site. However, in com-

M. Fiebig, Department of Applied Physics, The University of Tokyo, Tokyo 113-8656, Japan, and Japan Science and Technology Corporation (JST), Tokyo 171-0031, Japan.
K. Miyano, Department of Applied Physics, The University of Tokyo, Tokyo 113-8656, Japan.
Y. Tomioka, Joint Research Center for Atomic Technology (JRCAT), Tsukuba 305-0046, Japan.
Y. Tokura, Department of Applied Physics, The University of Tokyo, Tokyo 113-8656, Japan, and JRCAT, Tsukuba 305-0046, Japan.

*To whom correspondence should be addressed. E-mail: fiebig@ap.t.u-tokyo.ac.jp

pounds with relatively narrow conduction bandwidth, charge ordering—that is, real-space ordering of Mn^{3+} and Mn^{4+} species—competes with the FM double exchange between the localized spins of the Mn ions. Therefore, with decreasing temperature, transition occurs in which the charge carriers localize in a variety of structural and magnetic ordering patterns (*2*). In some of the perovskite manganites, the charge-ordered state can be transformed into a FM state again by application of external forces. This transformation is accompanied by a pronounced change in resistivity; in the presence of a magnetic field, it is termed "colossal magnetoresistance" (CMR) (*1*). $Pr_{1-x}Ca_xMnO_3$ is an example of CMR, as it shows insulating behavior over the whole composition (x) range because of the narrow bandwith of electrons assigned to the e_g orbital (*3*).

The ground state of $Pr_{0.7}Ca_{0.3}MnO_3$ exhibits charge-localizing real-space ordering of Mn^{3+} and Mn^{4+} ions that occurs at ~220 K; antiferromagnetic ordering occurs at ~130 K, and at ~115 K spin canting occurs (*4*). The compound can be driven back into the conducting metallic state upon application of a magnetic (*3*) or electric (*5*) field, high pressure (*6*), or exposure to x-rays (*7*) or visible light (*8*). The application of a magnetic field or high pressure causes the whole sample to undergo the phase transition when the external perturbation exceeds a critical value. In contrast, there is evidence that the application of an electric field, x-rays, or visible light results in an I-M transition that may not always affect the whole bulk of the sample. A nucleation of metallic patches that form one or more filamentary metallic paths may occur instead (*3, 5, 7*). The formation of current filaments generated by impurity breakdown is well known for the case of high-purity semiconducting layers (*9–11*). However, the breakdown model for semiconductors is not applicable to the CMR manganites because of their strong magnetic correlations. In this case, paths have not yet been observed and the existence of a "local phase transition" remains unclear.

We therefore applied an optical imaging technique to spatially resolve a $Pr_{0.7}Ca_{0.3}MnO_3$ single crystal undergoing a light-induced phase transition (Fig. 1). For this purpose, two pairs of gold electrodes were vacuum-evaporated onto the surface of the sample (size 4 mm by 4 mm by 1 mm), which had been grown, prepared, and annealed as described (*8, 12*). Both pairs of electrodes were separated by a straight 150-μm gap and wired as shown in Fig. 2A. The I-M transition was induced by illuminating the gap between the electrodes with 7-ns, 1064-nm laser pulses while applying a voltage of typically 10 to 100 V. The phase transition can only be induced if the laser spot fully covers the space between the electrodes (at an arbitrary position along this gap) while the laser-pulse energy exceeds a threshold value that is determined by the electric field between the electrodes and the laser wavelength (*8, 13*). Once the phase transition had occurred (Fig. 1), it remained stable as long as a current I was flowing between the electrodes, in which case the laser was turned off. The spatially resolved reflectivity of the sample was measured by illuminating it with light emitted from a Xe lamp that was spectrally narrowed by means of various narrow band-pass interference filters. The reflected light was projected onto a cooled charge-coupled device camera with a telephoto lens.

Three images of a section of the sample illuminated with light at $\lambda = 1000$ nm, with currents of 0, 10, and 100 mA flowing between the electrodes, are shown in Fig. 2, A to C. The change of reflectivity ΔR due to the flowing current was visualized by digitally subtracting the image of the conducting sample from the image of the insulating sample. For $I = 0$ mA (Fig. 2A), the sample remains in the insulating state and the difference image should not exhibit a variation of brightness at all. Nevertheless, small variations creating a three-dimensional effect are visible. These variations originate in tiny (<1 μm) shifts of the sample; during the time lapse between the two images, these shifts are caused by the stream of helium in the continuous-flow cryostat in which the sample is mounted. In the conducting state, however, a distinct change of reflectivity of the sample is observed along a well-localized path between the electrodes. This path is formed inside the region that had been illuminated by the laser pulse and generally remains pinned to its original position. In a few cases, spontaneous movement to another position could be observed, usually upon increasing I. However, these spontaneous shifts can be suppressed by using tine-shaped electrodes, where the magnitude of the electric field is higher and therefore more favorable for the phase transition in a well-defined region on the sample.

At $I = 10$ mA (Fig. 2B), the width of the

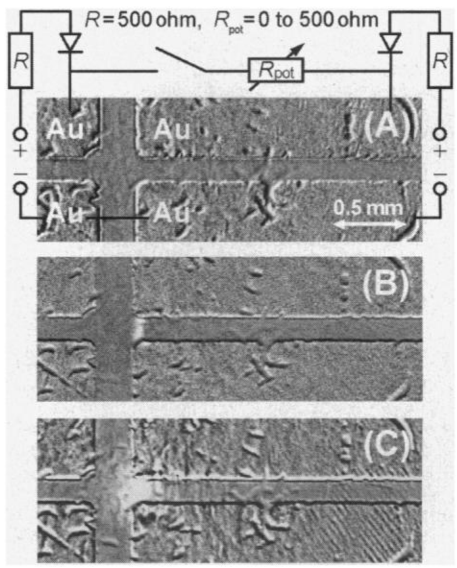

Fig. 2. Differential images of a $Pr_{0.7}Ca_{0.3}MnO_3$ sample with gold electrodes (Au) taken with light at $\lambda = 1000$ nm reflected from the sample surface. The sample at $T = 30$ K is in the insulating state at $I = 0$ mA (**A**) and in the conducting state at $I = 10$ mA (**B**) and $I = 100$ mA (**C**), respectively. At 1000 nm, the reflectivity of the sample is greater in the insulating than in the conducting state, so that white areas in the differential images denote the region where the phase transition has occured. A conducting metallic path can be generated at arbitrary positions along the gap between the electrodes by illuminating this position with the laser pulse while an electric field is applied between the electrodes. Here, the path was generated at the far left side of the electrodes to show how it spreads out into the surrounding material. The wiring of the sample is depicted in (A), with + and − indicating the poles of a regulated power supply.

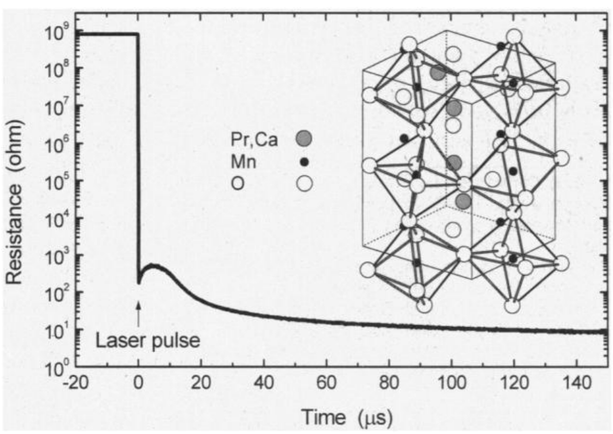

Fig. 1. The light-induced I-M transition in $Pr_{0.7}Ca_{0.3}MnO_3$. The sample resistance at T = 30 K upon illumination with a 7-ns, 1064-nm light pulse from a Nd–yttrium-aluminum-garnet laser is shown as a function of time. After the illumination (t = 0), a change of resistance of more than eight orders of magnitude occurs. If the current is limited with a regulated power supply, the phase transition can be monitored by the breakdown of the voltage applied to the sample. The inset shows the crystal structure of the compound.

path is about 30 μm. At lower current, it is even narrower and may actually become filamentary, but this is not resolved by the optical system. Upon an increase to $I = 100$ mA (Fig. 2C), the voltage drop U across the conducting path decreases, which indicates its unusual negative differential resistance dU/dI (*14*). The width of the path approaches 250 μm, and it exceeds 500 μm when I is further increased. The change of reflectivity occurs gradually, increasing toward the center of the path. Even though the width of the path is increasing by an order of magnitude, the change of reflectivity in the center is independent of the flowing current, hence the brightness of the paths in Fig. 2, B and C, is the same.

In the center, the material fully undergoes the phase transition even at low I. In the vicinity, metallic patches are created; their density decreases with increasing distance from the center, thus leading to a gradual change of reflectivity. If I is increased, the density of metallic patches is also increased while the region that has fully been transformed into the metallic state is swelling. If I is large enough, the metallic region in Fig. 2 is so expanded that even the space between the left pair of electrodes becomes conducting.

It could be argued that electric currents up to 100 mA may lead to considerable heating of the sample, which in turn could also lead to a change of reflectivity. However, the increase of temperature measured after the transition does not exceed ~1 K because the sample is constantly cooled by the flowing helium gas. Local heating effects can also be neglected: They would increase with higher current, whereas the observed change of reflectivity is independent of I. Local heating by the laser pulse can also be excluded (*8*, *14*) as a possible origin for the observed change of resistivity (Fig. 1).

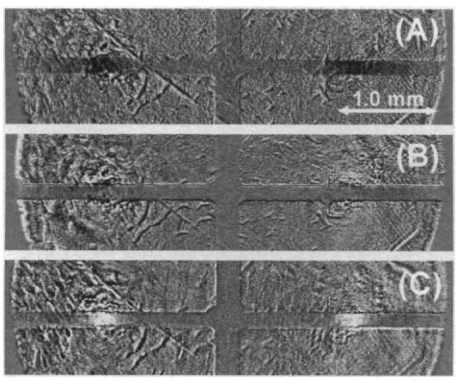

Fig. 3. Differential reflection image of a $Pr_{0.7}Ca_{0.3}MnO_3$ sample at $T = 30$ K and $I = 100$ mA, taken with light at (**A**) 400 nm, (**B**) 680 nm, and (**C**) 1000 nm. The images represent the change of reflectivity of the insulating sample with respect to the conducting sample.

Three images of the sample, taken at wavelengths of 400, 680, and 1000 nm, are shown in Fig. 3, A to C. At $\lambda = 400$ nm, the reflectivity of the insulating sample is lower than that of the metallic region ($\Delta R = -5\%$), which appears black in Fig. 3A. At $\lambda = 1000$ nm, however, the reflectivity of the insulating sample is greater than that of the metallic region ($\Delta R = +12\%$), which thus appears white in Fig. 3C. Low reflectivity of infrared (IR) light is most unusual for "ordinary" metals. In $Pr_{0.7}Ca_{0.3}MnO_3$, the reflectivity in the metallic state in the near-IR spectral range should, however, be small because of the small energy of the pseudo plasma edge (*15*). Our finding of lower reflectivity of the metallic sample in the near-IR is consistent with results of the magnetic field–induced I-M transition in a similar related compound (*15*).

The gradual change of reflectivity near the path might be attributed to the deformation accompanying the phase transition, not the transition itself. In that case, however, ΔR should be independent of the wavelength of the reflected light, which contrasts our observations. Moreover, the reflectivity of the gold should also change as a consequence of the formation of dents or bulges on the surface that scatter the light. The latter has in fact been observed at the crossover wavelength $\lambda_c = 680$ nm (Fig. 3B). For other wavelengths, the effect is negligible even at high currents.

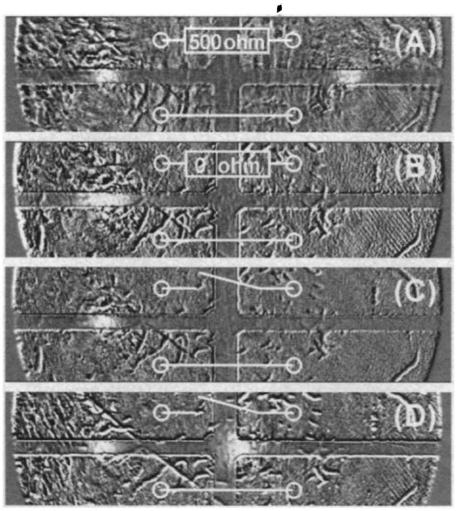

Fig. 4. Differential reflection image of a $Pr_{0.7}Ca_{0.3}MnO_3$ sample at $T = 30$ K, taken with light at $\lambda = 1000$ nm. The competition and induction of two 100-mA paths is shown with additional graphics depicting the wiring of the two pairs of electrodes. (**A**) Two paths after connection via a 500-ohm resistance. (**B**) After setting the resistance to 0 ohm; one of the paths has vanished. (**C**) After disconnecting the electrodes again. (**D**) After increasing the voltage across the now insulating gap between the right pair of electrodes until an I-M transition is induced without light.

Once a metallic path has been created, it is not possible to generate a second path between the same pair of electrodes. Obviously, the current is centered on a single low-resistivity path after this has been opened. To study the competition of two conducting paths in detail, we prepared a sample with two independent pairs of electrodes. A metallic path was light-induced at either pair. Afterward, the electrodes were connected by a variable resistance (Fig. 2) and the behavior of the paths was monitored by the differential reflection technique described above.

In Fig. 4A, the electrodes have been connected via a 500-ohm resistance, which leaves the two conducting paths ($I = 100$ mA) unchanged. In Fig. 4B, the resistance between the electrodes has been set to zero. As a consequence, the right path has vanished, and the left part has swollen because the total current of 200 mA is now flowing between the left pair of electrodes. (The disappearance of one path can only be detected from the corresponding change of reflectivity, not by monitoring the power supplies.) By disconnecting the anodes again (Fig. 4C), the current flowing through the remaining path has been reduced to 100 mA. If the voltage applied to the now insulating right-hand side is increased again, an I-M transition is once more induced, but this time without the use of light (Fig. 4D). The path is induced at the closest possible distance to the left path (1.3 mm) with a "trigger voltage" $V_{ind} = 60$ V at $T = 30$ K. The path cannot be induced, even at 150 V, in the absence of the first path.

Although connected, two conducting paths can be maintained as long as the resistance inserted between them exceeds a critical value R_c. This value distinctly depends on the current flowing through the paths. For $I = 10$ mA we find $R_c > 1000$ ohms, whereas for $I = 100$ mA we get $R_c < 10$ ohms. For $R < R_c$ the path through which the lower current is flowing will vanish. If approximately the same current is flowing through either path, minimal deviations prevail and it cannot be predicted which path will vanish upon connection. Thus, the stability of a path is proportional to its corresponding current. The instability associated with two competing paths is a direct consequence of the unusual non-ohmic resistance of the conducting path, which decreases with increasing current (*8*, *12*). Usually this favors the formation of a single path out of two because the increase of current in one of the paths leads to a lower resistance. Two paths can be maintained only if the connecting resistance, which must be surmounted to encounter the energetic minimum with one path only, is larger than the decrease in resistance because of an increase of current in the path with the higher current.

The induction of a conducting path in the absence of light is clearly triggered by the presence of the first path, because at constant temperature V_{ind} decreases with higher current flow through the conducting path and with closer proximity to the first path. The distance across which a metallic path can be induced can be much greater than the distance at which a change of reflectivity due to the formation of metallic patches can be detected. The trigger voltage is distinctly dependent on temperature, whereas the width of a conducting path is not.

The successful visualization of the local photoinduced I-M transition by the depicted differential reflection technique opens the way for a variety of further experimental studies. Our observations already indicate that the requirements for creating the transition and maintaining the transition are fundamentally different. With respect to applications, the local I-M transition is a tool for switching the resistivity of a material by many orders of magnitude in a controllable and observable way. The generation and removal of one or more conducting paths at arbitrarily chosen spots of a sample is performed by the appropriate choice of external parameters and monitored with visible light. These features suggest an application of the local photoinduced I-M transition in the construction of optical switching devices. In the experiment, a gap of 150 μm between the electrodes was chosen to simplify the imaging, and a regulated dc power supply was used for experimental convenience. With a gap width of 25 μm, however, the applied voltage could be reduced to the order of 1 V, which can be provided by ordinary power supplies.

REFERENCES AND NOTES

1. A. J. Millis, *Nature* **392**, 147 (1998).
2. Z. Jirak, S. Krupicka, Z. Simsa, M. Dlouha, S. Vratislav, *J. Magn. Magn. Mater.* **53**, 153 (1985).
3. Y. Tomioka, A. Asamitsu, H. Kuwahara, Y. Morimoto, Y. Tokura, *Phys. Rev. B* **53**, R1689 (1996).
4. H. Yoshisawa, H. Kawano, Y. Tokura, *ibid.* **52**, 13145 (1995).
5. A. Asamitsu, Y. Tomioka, H. Kuwahara, Y. Tokura, *Nature* **388**, 50 (1997).
6. Y. Morimoto, H. Kuwahara, Y. Tomioka, Y. Tokura, *Phys. Rev. B* **55**, 7549 (1997).
7. V. Kiryukhin *et al.*, *Nature* **386**, 813 (1997).
8. K. Miyano, T. Tanaka, Y. Tomioka, Y. Tokura, *Phys. Rev. Lett.* **78**, 4257 (1997).
9. W. Eberle *et al.*, *Appl. Phys. Lett.* **68**, 3329 (1996).
10. W. Prettl, in *Nonlinear Physics of Complex Systems. Current Status and Future Trends*, J. Parisi, S. C. Muller, W. Zimmermann, Eds. (Springer-Verlag, Berlin, 1996), pp. 341–352.
11. N. Balkan, B. K. Ridley, A. J. Vickers, Eds., *Negative Differential Resistance and Instabilities in 2D Semiconductors*, NATO Advanced Research Workshop, Il Ciocco, Lucca, Italy (NATO ASI Series, Overijse, Netherlands, 1992).
12. Y. Tomioka, A. Asamitsu, Y. Morimoto, Y. Tokura, *J. Phys. Soc. Jpn.* **64**, 3626 (1995).
13. T. Mori *et al.*, *ibid.* **66**, 3570 (1997).
14. K. Ogawa, W. Wei, K. Miyano, Y. Tomioka, Y. Tokura, *Phys. Rev. B*, in press.
15. Y. Okimoto, Y. Tomioka, Y. Onose, Y. Otsuka, Y. Tokura, *Phys. Rev. B*, in press.

16. Supported in part by the Core Research for Evolutional Science and Technology (CREST) of JST, and by a Grant-in-Aid for Center of Excellence Research from the Ministry of Education, Science, Sports and Culture of Japan. The work at JRCAT was supported by The New Energy and Industrial Technology Development Organization.

5 March 1998; accepted 7 May 1998

Call Duration as an Indicator of Genetic Quality in Male Gray Tree Frogs

Allison M. Welch,* Raymond D. Semlitsch, H. Carl Gerhardt

The "good genes" hypothesis predicts that mating preferences enable females to select mates of superior genetic quality. The genetic consequences of the preference shown by female gray tree frogs for long-duration calls were evaluated by comparing the performance of maternal half-siblings sired by males with different call durations. Offspring of male gray tree frogs that produced long calls showed better performance during larval and juvenile stages than did offspring of males that produced short calls. These data suggest that call duration can function as a reliable indicator of heritable genetic quality.

The "good genes" model of sexual selection predicts that some attributes of male courtship displays advertise genetic quality. Preferences for such attributes should allow females to mate with high-quality males and thereby benefit indirectly through enhanced quality of offspring (*1*). Although the good genes hypothesis has been tested several times (*2*), few studies have provided direct genetic evidence supporting this hypothesis (*3*). Only one such study involved a species in which females cannot benefit directly from their choice of mates (*4*). Because selection for direct benefits such as courtship feeding or parental care should overwhelm any selection for indirect (genetic) benefits (*5*), the role of good genes selection in the evolution and maintenance of female preferences is best tested in species in which females do not benefit directly from mate choice.

Female gray tree frogs (*Hyla versicolor*) strongly prefer male advertisement calls of long duration in laboratory experiments (*6*, *7*). In the field, females freely initiate matings with calling males and do not always choose the first male encountered (*7*). Because males do not defend oviposition sites, offer nuptial gifts, or contribute parental care (*8*, *9*), and no difference has been found in fertilization success as a function of call duration (*10*), there are no apparent direct benefits of a female's mate choice. We therefore predicted that females selecting mates with long calls should benefit indirectly through increased fitness of offspring. This prediction can be tested by evaluating the relation between paternal call duration and the genetic quality of offspring.

Male gray tree frog advertisement calls consist of rapidly repeated pulses. In dense choruses and in response to playbacks, males tend to increase call duration by increasing the number of pulses per call (*11*, *12*). Nonetheless, some males consistently produce longer calls than others in the same acoustic environment (*7*, *12–14*). Although long calls are usually produced at slow rates, thereby keeping aerobic metabolic costs relatively constant (*11*, *14*), males that produce long calls spend less time calling per night (*11*) and attend fewer choruses per season (*8*) than males that produce short calls. Long calls thus appear to impose higher nonaerobic costs than short calls. Call duration may, therefore, be an honest indicator of male genetic quality.

We tested whether call duration indicates heritable genetic quality by using maternal half-siblingships (half-sibships) to compare the performance of different males' offspring while experimentally controlling for all maternal effects. Maternal half-sibships were generated by artificially crossing each female with two males that had been giving calls of distinctly different durations in the same social environment (Table 1). Thus, within each maternal half-sibship, one sibship was sired by a male with calls of longer duration than the male siring the other sibship. Because call duration varies with chorus density, males' calls must be assessed in the same social context in order to be validly compared. Thus, in 1995 we selected nine sets of two males that had

Division of Biological Sciences, University of Missouri, Columbia, MO 65211, USA.

*To whom correspondence should be addressed. E-mail: awelch@biosci.mbp.missouri.edu